Multibaseline InSAR Layover Detection Based on Local Frequency and Eigenvalue

Huaping Xu, *Member, IEEE*, Siyuan Wang, Shuo Li, Guobing Zeng, Zhenwan You, and Wei Li

***Abstract*—Layover detection has long been the focus of attention for interferometric synthetic aperture radar (InSAR) data processing. As for the existing layover detection methods, most of them are applied to single-baseline scenarios. Since multibaseline InSAR provides more image samples, the performance of layover detection can be further improved. In this article, a joint detection method of layover is proposed on the basis of local frequency and eigenvalue of multibaseline InSAR. To obtain a precise local frequency, maximum likelihood estimation is performed for flattened interferometric phase fusion and removing the reference terrain phase is chosen to ensure the proportionality of flattened phase to the baseline length. Adaptive image selection based on coherence is proposed to obtain a distinct eigenvalue. Then, the joint detection method is elaborated on. Based on the results of local frequency estimation and eigenvalue decomposition, precise thresholds are set for joint detection, and joint judgment is made by combining the layover detected by local frequency, the layover detected by eigenvalue, and the thresholds. Finally, the proposed method is validated through comparative experiments on simulated data and real data. Both theoretical analysis and experimental results show the feasibility and superiority of the proposed method.**

***Index Terms*—Eigenvalue, InSAR, layover detection, local frequency, multibaseline.**

I. Introduction

SYNTHETIC aperture radar (SAR) exhibits excellent advantages in topographic mapping, e.g., all-weather, all-day, and the capability to collect topographic information from the areas with poor measurement conditions [1]. Interferometric synthetic aperture radar (InSAR) is an important branch of SAR development. It provides high precision elevation information and surface deformation through the phase difference of single look complex (SLC) SAR images acquired by multiple antennas or multiple passes of a single antenna. The elevation information and surface deformation have been widely applied in agriculture, forestry, geology, ocean, disasters, and military [2]–[5]. Multibaseline InSAR employs no less than three SAR complex images to form no less than two baseline interferograms. Thus, it holds massive potential for boosting the information content in the multidimensional data space [6]–[11].

Regarding SLC SAR images, a series of processing steps are required to obtain the final elevation information and to identify surface deformation. The filtering and unwrapping of interferometric phase are the critical steps in InSAR processing. However, due to the inherent side-view imaging geometry of SAR, there are inevitably problematic areas with severely impaired interferometric phase, which can cause the phase filtering and unwrapping performance to deteriorate significantly. Layover is a common phenomenon arising from the superposition of radar echoes derived from different scattering cells into the same range-azimuth resolution unit [12]. Since the layover area is not capable of being phase filtered and unwrapped correctly, it probably provides invalid, or in some circumstances even false information. Furthermore, it may transmit misinformation to the surrounding pixels, thus causing large-area errors with phase filtering and unwrapping. In addition, some multibaseline InSAR technologies are applied to solve the problems caused by layover [13], [14]. If the proposed solutions are only performed on layover pixels, the computational efficiency will be improved considerably. Therefore, it is necessary to detect and mark layover pixels in advance. It would avoid executing InSAR phase filtering and unwrapping on these pixels. Besides, the layover solution could be performed only on them in the following process.

For the prior literature on layover detection, the focus is placed mainly on single-baseline InSAR technique. According to layover mechanism of SAR image, it exhibits distinctive characteristics in the amplitude and phase of layover pixels, which derives various detection methods. Soergel *et al.* [15] proposed the amplitude segmentation for the first time. Based on the high amplitude of the layover area, a threshold is set to segment the SAR image. The efficiency and outcome of segmentation show slight variation depending on the threshold and the image segmentation algorithm applied, such as the unsupervised image segmentation algorithm suggested by He [16], the CFAR algorithm adopted by Qin [17], the OSTU method applied by Yu [18], etc. Besides, Prati *et al.* [19] demonstrated that slopes could cause spectral shift of SAR interferogram, which constitutes the theoretical basis for the layover detection based on local frequency. Gatelli *et al.* [20] suggested that the spectrum shift theory is applicable to separate layover regions from nonlayover regions partially for application in ERS images. Petit *et al.* [21] verified the feasibility of spectrum shift theory using simulated

Manuscript received April 24, 2021; revised June 12, 2021 and August 2, 2021; accepted October 1, 2021. Date of publication October 14, 2021; date of current version October 28, 2021. This work was supported by the Shanghai Aerospace Science and Technology Innovation Fund under Grant SAST2019-026. *(Corresponding author: Huaping Xu.)*

Huaping Xu, Siyuan Wang, Shuo Li, Guobing Zeng, and Zhenwan You are with the School of Electronic and Information Engineering, Beihang University, Beijing 100191, China (e-mail: xuhuaping@buaa.edu.cn; siyuanwang0822@buaa.edu.cn; shuo201@buaa.edu.cn; zengguobing@buaa.edu.cn; youzhenwan@buaa.edu.cn).

Wei Li is with the Shanghai Lizheng Satellite Application Technology Company, Ltd, Shanghai 201100, China (e-mail: liwei20rth@139.com).

Digital Object Identifier 10.1109/JSTARS.2021.3120007

images to process urban SAR images. In 2016, Liu *et al.* [22] proposed to extract the layover area of high-rise buildings by quantifying the spectral shift. Similar to the principle of layover detection based on local frequency, Rossi *et al.* [23] put forward a layover area recognition algorithm in urban areas, using the gradient of the unwrapped phase. In addition to the above methods, based on the estimation of the number of signal sources, another kind of layover detection methods includes eigenvalue decomposition and information theoretic criteria. In 1985, Max [24] proposed the main principle of eigenvalue decomposition and information theory criteria. Zou *et al.* [25] applied information theory criteria to detect the layover area in spaceborne single-baseline InSAR.

The detection methods based on single feature suffer from high false alarm and low accuracy. Despite many features (amplitude, local frequency, eigenvalue, etc.) in the layover area that exhibit different properties from the normal area, some features are susceptible to noise, while some features are not unique to the layover area. Consequently, the extraction of features is not as precise as required, so does the layover detection. For this reason, multifeature detection methods have been proposed, combining several kinds of features. In order to solve the problem that eigenvalues are easily affected by noise, Chen *et al.* [26] set eigenvalue thresholds using amplitude information and noise variance. In order to distinguish layover from other areas with a local frequency less than zero, Du *et al.* [27] performed the amplitude segmentation for all the pixels with a local frequency less than zero, and then mark those with an amplitude greater than two times the average amplitude as layover. The authors' multifeature joint detection method proposed in 2020 [28] for single-baseline InSAR has produced the most significant detection effect among the existing layover detection methods.

Multiple features can be used to improve the precision of layover detection to some extent. However, there are only master and slave SAR images in the single-baseline InSAR, as a result of which the extraction of each feature is not as precise as expected. Multibaseline InSAR provides more image samples, thus further improving the precision of the feature estimation applied for layover detection. Among the published articles, only Chen *et al.* [26] in our research team have conducted study on layover detection of multibaseline InSAR, but the detection performance of their method is limited because only eigenvalue is used and all available images are used to estimate the eigenvalue without data choosing.

In this article, a joint detection method is proposed by combining local frequency and eigenvalue of multibaseline InSAR data. Based on the results of local frequency estimation and eigenvalue decomposition of multibaseline InSAR, the precise thresholds are determined for joint detection. Then, joint judgment is performed by combining the layover detected by local frequency, the layover detected by eigenvalue, and the thresholds.

The rest of this article is organized as follows. In Section II, the local frequency estimation and eigenvalue decomposition of multibaseline InSAR are presented. The proposed layover joint detection method of multibaseline InSAR is elaborated on in Section III. In Section IV, three experiments are conducted and the experimental results validate the proposed method.

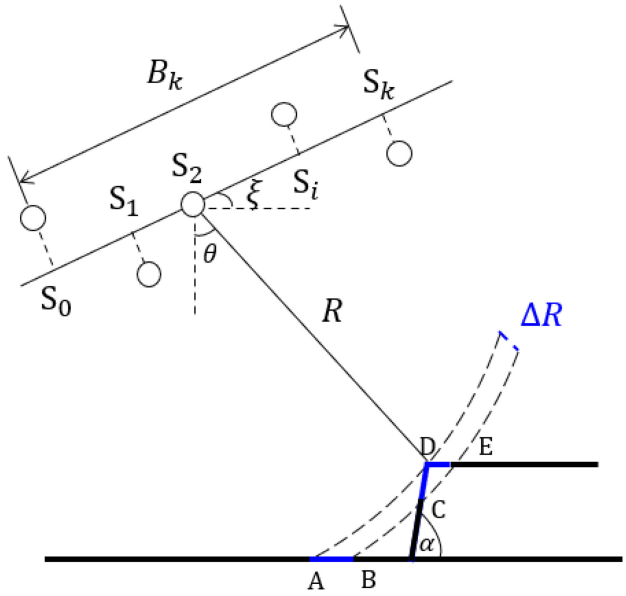

Fig. 1. Schematic diagram of the principle of multibaseline InSAR on a fixed azimuth. The platform flies in the direction into the article. The multibaseline data can be compensated to the positions S_0, S_1, S_2, ..., S_i, ..., S_k, so that all baselines have the same baseline inclination, denoted by ξ. B_k denotes the longest baseline. θ denotes the look angle. R denotes the slant range. The area enclosed by the dashed line is a resolution unit. Areas AB, CD, and DE are projected in a single pixel of the SAR image, forming layover.

II. Feature Extraction Using Multiple Baselines

Different features are used to identify layover pixels in existing methods. However, unwrapped phase is rarely used in layover detection due to the difficulty of phase unwrapping. And the amplitude has a very high false alarm in layover detection because numerous factors affect the amplitude [26]. Moreover, correlation coefficient is usually used to detect shadow, but the coherence analysis of layover area is complicated [27]. In contrast, local frequency and eigenvalue are relatively precise and accurate. Specifically, local frequency is excellent in distinguishing between normal and abnormal areas; eigenvalue determines the number of signal sources well, distinguishing layover area from the other areas. Therefore, our multibaseline layover detection method is proposed by a joint feature detection based on local frequency and eigenvalue.

In the single-baseline InSAR, there are only master and slave images. Under this condition, the estimation of local frequency and the eigenvalue decomposition are greatly affected by noise. Conversely, more image samples could be available with multibaseline InSAR, and therefore more precise local frequencies and eigenvalues can be provided. Hence, more accurate layover detection can be expected.

The following part first presents the multibaseline signal model. Then, the multibaseline local frequency estimation and multibaseline eigenvalue decomposition are introduced.

A. Multibaseline Signal Model

Fig. 1 is a schematic diagram of the principle of multibaseline InSAR on a fixed azimuth. The platform flies in the direction into

the article. Assuming that the multibaseline InSAR has $k+1$ antennas in total, the multibaseline data can be compensated to the positions S_0, S_1, S_2, ..., S_i, ..., S_k, so that all baselines have the same baseline inclination, denoted by ξ. B_k denotes the longest baseline. θ denotes the look angle. R denotes the slant range. The area enclosed by the dashed line is a resolution unit, and all objects located in it will be imaged as a single pixel in the final SAR image. In Fig. 1, areas AB, CD, and DE are projected in a single pixel of the SAR image, forming layover. It is well known that interferometry can only be executed for SAR images obtained with slight incidence differences [29]. Hence, it can be assumed that the layover areas under different baselines are approximately the same.

The SLC SAR image obtained by the antenna S_0 is appointed as the master image. Respectively, the image obtained by S_i is coregistered to the master image, and the interferometric phase ϕ_i acquired from the interferogram of the master image and the image obtained by S_i is [30]:

$$\phi_i = -\frac{4\pi}{\lambda} B_i \sin(\theta - \xi),\ i = 1, 2, \ldots, k \tag{1}$$

where λ denotes the wavelength.

B. Local Frequency Estimation of Multibaseline InSAR

Spatial baseline is an important parameter for InSAR. Its length impacts the interferometric phase accuracy and precision. The longer spatial baseline interferometric phase implies higher height estimation accuracy because of a minor height ambiguity, which is conducive to reflect the detailed terrain. However, under the same temporal baseline, it has lower precision because the longer spatial baseline leads to more baseline decorrelation. Vice versa, the shorter spatial baseline interferometric phase has higher precision due to its high coherence. However, it only reflects coarser terrain because of the larger height ambiguity. To simplify the expression, the baseline all denotes spatial baseline when there is no special illustration in the following contents.

Multibaseline InSAR provides more image samples and helps to improve parameters estimation in SAR interferograms. Therefore, the phases of multibaseline InSAR could be fused to improve interferometric phase estimation both in accuracy and precision. In this article, the maximum likelihood estimation is used to fuse multibaseline InSAR data. The fusion takes advantage of the accurate long-baseline interferometric phase and the precise short-baseline interferometric phase. Thus, the process could provide a more precise fused phase in the long-baseline frame [31]. Thereby, the local frequency estimation is improved by using a fused interferometric phase.

The existing maximum likelihood fusion is implemented on the interferometric phase [32]. Layover detection is usually performed on the flattened interferometric phase. The term *flattened* indicates that the flat-earth phases of the wrapped phases have been removed. Hence, it is expected to achieve the maximum likelihood fusion on the flattened phase directly. There are many approaches to remove the flat-earth phase, such as the method using the coarse digital elevation model (DEM), the method using local frequency, and the method of removing the reference terrain phase [33]. In this article, the method of removing the reference terrain phase is chosen to ensure that the flattened interferometric phase is still proportional to the baseline length and the premise of maximum likelihood fusion is not wrecked.

According to Gatelli *et al.* [20], the layover area could be detected by analyzing the sign of the local frequency in the range direction of the interferometric phase. For local frequency estimation, the method in [34] is used in this article. Concretely, the two-dimensional fast Fourier transform (2-D FFT) is first performed. Then, the Chirp-z transform (CZT) is applied to improve the estimation precision of the local frequency with a small computational cost.

The local frequency estimation of multibaseline InSAR described below is divided into two steps: the interferometric phase fusion using maximum likelihood estimation and the local frequency estimation using 2-D FFT and CZT.

1) Interferometric Phase Fusion Using Maximum Likelihood Estimation: Maximum likelihood estimation fuses the interferometric phases of multibaseline InSAR by looking for the maximum of their likelihood functions. The function is constructed by normalized phase probability density function (pdf). The fused interferometric phase in the reference baseline frame is obtained by extracting the phase value corresponding to the maximum of the likelihood function. The longest baseline B_k is usually chosen as the reference baseline, and its interferometric phase ϕ_k is chosen as the reference phase due to its strong ability to reflect finer terrain.

The normalized phase pdf is on the basis that the interferometric phase is proportional to the baseline length. Layover detection is usually performed on the flattened interferometric phase. Thus, the proportionality of the flattened phase to the baseline length should be held when maximum likelihood estimation is executed on the flattened phase.

As mentioned above, the method of removing the reference terrain phase is chosen to implement flat-earth phase removing. The following paragraphs prove that the flattened phase is still proportional to baseline length.

Fig. 2 is the interferometric configuration for target *P*. The platform flies in the direction into the article. P' is a point on the reference terrain with the same slant range as P. The height difference between P and P' *is* ΔZ. The look angle change caused by ΔZ is $\Delta\theta_Z$.

According to (1), the interferometric phase $\phi_{\mathrm{P}'}$ and ϕ_{P} are expressed as follows:

$$\phi_{\mathrm{P}'} = -\frac{4\pi}{\lambda} B \sin(\theta - \xi) \tag{2}$$

$$\phi_{\mathrm{P}} = -\frac{4\pi}{\lambda} B \sin(\theta + \Delta\theta_Z - \xi). \tag{3}$$

The flattened phase obtained by removing the reference terrain phase is

$$\begin{aligned}\phi_f = \phi_{\mathrm{P}} - \phi_{\mathrm{P}'} &= -\frac{4\pi}{\lambda} B \left[\sin(\theta + \Delta\theta_Z - \xi) - \sin(\theta - \xi)\right] \\ &= -\frac{4\pi}{\lambda} B \cos(\theta - \xi)\, \Delta\theta_Z.\end{aligned} \tag{4}$$

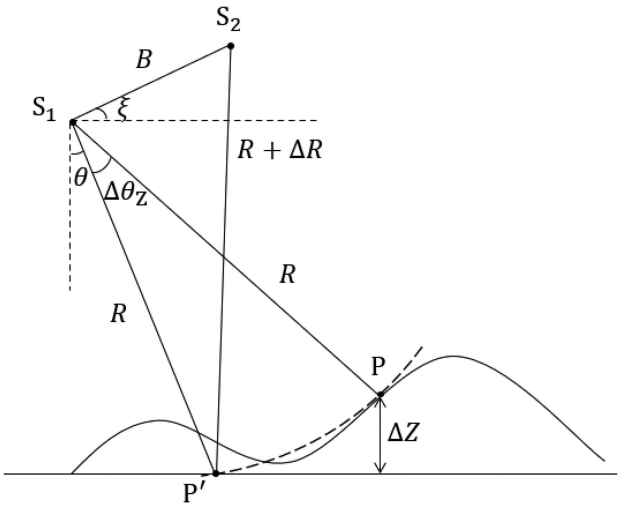

Fig. 2. Interferometric configuration for target P. The platform flies in the direction into the article. P' is a point on the reference terrain with the same slope range as P. The height difference between P and P' is ΔZ. The look angle change caused by ΔZ is $\Delta\theta_Z$.

It is shown in (4) that ϕ_f is still proportional to the baseline length. Therefore, the maximum likelihood fusion of multibaseline InSAR can be executed on the flattened phase, and the normalized pdf of the flattened interferometric phase $\phi_{i,f}$ could be constructed as [32]

$$\begin{aligned}&\mathrm{pdf}_{\mathrm{norm}}\ (\phi_{i,f}|\phi_{k0,f}) = \frac{1}{2\pi}\ \frac{1-|\gamma_i|^2}{1-|\gamma_i|^2\cos^2(\phi_{i,f}-\eta_i\phi_{k0,f})}\\ &\times\left\{1+\frac{|\gamma_i|\cos(\phi_{i,f}-\eta_i\phi_{k0,f})\arccos[-|\gamma_i|\cos(\phi_{i,f}-\eta_i\phi_{k0,f})]}{\sqrt{1-|\gamma_i|^2\cos^2(\phi_{i,f}-\eta_i\phi_{k0,f})}}\right\}\end{aligned} \tag{5}$$

where $\phi_{k0,f}$ denotes the unknown flattened real phase, γ_i represents the complex correlation coefficient, and η_i denotes the ratio between other baselines and reference baseline:

$$\eta_i = \frac{B_i}{B_k}. \tag{6}$$

Assuming that the multibaseline interferometric phases are independent mutually, the likelihood function can be expressed by the product of the normalized phase pdf of k interferometric phases. The phase corresponding to the peak of the likelihood function is the fused interferometric phase in the reference baseline frame.

2) Local Frequency Estimation Using 2-D FFT and CZT [34]: According to Zhu [34], the local frequency estimated by the 2-D FFT is maximum likelihood. After the flattened interferometric phase fusion in Section II-B-1, 2-D FFT is performed to extract the local frequency in the range direction. The main idea is to simulate the interferometric phase in a small window ϕ_w with a 2-D single-frequency signal.

The 2-D frequency spectrum of the phase in the window is achieved through 32×32 points FFT. The peak of the 2-D spectrum should appear at the position corresponding to the 2-D local frequencies $f_{\mathrm{a,\ FFT}}(m,n)$ and $f_{\mathrm{r,FFT}}(m,n)$. Layover detection only cares about the local frequency in the range direction. Compared with zero padding FFT, CZT could perform fine estimation of the main lobe with a smaller computational cost. Thus, 96 points CZT is performed on $f_{\mathrm{r,FFT}}(m,n)$ to get $f_{\mathrm{r,\ CZT}}(m,n)$, improving the estimation precision of local frequency in the range direction. $f_{\mathrm{r,\ CZT}}(m,n)$ will be used for layover detection.

C. Eigenvalue Decomposition of Multibaseline InSAR

Eigenvalue decomposition and information theoretic criteria are often used to estimate the number of signal sources in the array signal processing. It could be used for layover detection [26] because the layover area is formed by the superposition of radar echoes from different ground scattering areas, and there is more than one signal source. There is only one signal source in the normal area. And in the shadow area, there is no signal source, and what appears is thermal noise.

There is a cross-blur between signal eigenvalues and noise eigenvalues in single-baseline eigenvalue decomposition due to the small number of image samples. Multibaseline InSAR can improve the estimation precision of eigenvalues by increasing the number of samples.

There are very few researches on multibaseline InSAR layover detection using eigenvalue decomposition. Although Chen *et al.* [26] implemented multibaseline InSAR layover detection using eigenvalue decomposition, they did not analyze the influence of interferogram quality on the eigenvalue decomposition and added all available images to the operation, which may degrade the eigenvalue estimation in some cases.

According to probability theory, the increase of sample number improves the estimation precision of eigenvalues. However, it is based on the premise that the multibaseline data has a similar quality. In practice, blindly increasing the number of SLC SAR images used may inhibit eigenvalue deposition. Noise in complex interferograms can be described as additive white Gaussian noise, and its standard deviation depends on the coherence [35]. Interferometric phase noise causes the diffusion of large eigenvalues to small eigenvalues [25]. Samples with weak coherence may damage the estimation of the number of signal sources.

Thus, before eigenvalue decomposition of multibaseline InSAR, it is necessary to select the suitable SLC SAR images, aiming to maximize the samples used while considering the coherence. The coherence is closely related to the ground scene, and thus different images are selected for different areas. It is called adaptive image selection. Then eigenvalue decomposition is carried out only using the selected images.

The eigenvalue decomposition of multibaseline InSAR described below is divided into two steps: the adaptive image selection and the eigenvalue decomposition using selected images.

1) Adaptive Selection of SLC SAR Images: The master image is partitioned into several areas with prominent layover features according to the SAR amplitude image. For every area, its image set for eigenvalue decomposition is selected according to its coherence, respectively. The correlation coefficient of the area is chosen as the vital factor for image selection. When the partitioned area is large, the real correlation coefficient is applied [36]; otherwise, the complex correlation coefficient is calculated [37]. The amplitude of the correlation coefficient is $[0,\ 1]$. If it

is equal to 0, the two images are entirely uncorrelated; if it is equal to 1, the two images are wholly correlated.

Generally, interferometric fringe can be well achieved with a correlation coefficient above 0.6. Thus, the selection threshold is determined by the statistical histogram of correlation coefficients above 0.6, i.e., finding the double peaks of the histogram and taking the correlation coefficient located in the trough of the double peaks as the selection threshold. The SLC SAR images with the correlation coefficient greater than the threshold will join in eigenvalue decomposition. 0.6 is an empirical value and can be adjusted with the application scenarios.

2) Eigenvalue Decomposition [24], [26]: Assuming that p is the number of SLC SAR images adaptively selected for one area. For instance, there are only master and slave images for the single-baseline InSAR, so $p = 2$. The signal model constructed for the pixel (m, n) is

$$\boldsymbol{s}\ (m,n) = \boldsymbol{L} * \boldsymbol{c}\,(m,n) + \boldsymbol{n}\,(m,n) \tag{7}$$

where $\boldsymbol{s}(m,n)$ is a $p \times 1$ complex vector and denotes the signal received at pixel (m,n); $\boldsymbol{c}(m,n)$ is a $q \times 1$ complex vector and denotes the signal component of $\boldsymbol{s}(m,n)$, where q is the number of uncorrelated signals received at pixel (m,n); $\boldsymbol{n}(m,n)$ is a $p \times 1$ complex vector and indicates noise component; $\boldsymbol{L}$ is a $p \times q$ complex common matrix making the equation reasonable. Specifically, $\boldsymbol{s}(m,n)$ is assumed to be an ergodic Gaussian process with zero mean and a positive definite covariance matrix. $\boldsymbol{n}(m,n)$ is also an ergodic Gaussian process, independent of the signals, with zero mean and variance σ^2.

Then, eigenvalue decomposition is performed on the signal covariance matrix $\boldsymbol{R}(m,n) = E\{\boldsymbol{s}(m,n)\boldsymbol{s}(m,n)^H\}$ to obtain the eigenvalue vector of pixel (m,n):

$$\boldsymbol{R}\ (m,n) = \boldsymbol{U}\,(m,n)\,\boldsymbol{\Lambda}\,(m,n)\,\boldsymbol{U}^{\boldsymbol{H}}\,(m,n) \tag{8}$$

where $\boldsymbol{U}(m,n)$ is a $p \times p$ matrix composed of the eigenvectors of $\boldsymbol{R}(m,n)$; $\boldsymbol{\Lambda}(m,n)$ is a diagonal array, and the value on the diagonal represents p eigenvalues of $\boldsymbol{R}(m,n)$.

The p eigenvalues are arranged in descending order to form the eigenvalue vector $\boldsymbol{\lambda}(m,n)$ for pixel (m,n). Then, the former q larger eigenvalues are provided by both signal and noise, while the latter $p-q$ smaller eigenvalues are provided by noise only [26]. The details to determine q are presented in the following sections. Finally, the obtained eigenvalues will be used for layover detection.

III. Joint Detection of Layover With Multibaseline SAR Interferograms

The layover detection only using local frequency performs well in distinguishing between normal and abnormal areas [28]. However, it needs the SAR amplitude image to extract the layover area, and the result of layover detection is greatly affected by the amplitude threshold. Furthermore, in the layover detection only using eigenvalue, the eigenvalue threshold is determined by experience, which is not adaptive to the scene. So we propose that the layover detection result using local frequency can be regarded as prior information to calculate the threshold required by the layover detection using eigenvalue. Then, local frequency and eigenvalue are combined for a joint layover detection.

In this section, a novel layover detection method is proposed by using multibaseline interferometry and combing local frequency and eigenvalue. The principle is shown as follows.

Assuming that the amplitude of the master image s_0 at pixel (m,n) is $A(m,n)$. The average of the whole image's amplitude is $\bar{A}$. Then, the layover area L_1 and the normal area N marked by local frequency are shown as

$$L_1 = \left\{(m,n) \in s_0 | f_{\mathrm{r,\ CZT}}\,(m,n) < 0\ and\ A\,(m,n) > 2\bar{A}\right\} \tag{9}$$

$$N\ = \{(m,n) \in s_0 | f_{\mathrm{r,\ CZT}}\,(m,n) \geq 0\}\,. \tag{10}$$

The layover pixel has more than one larger eigenvalue, while the normal area has only one larger eigenvalue. Consequently, the eigenvalue decomposition is focused on the second largest eigenvalue $\lambda_2(m,n)$. The thresholds for joint detection σ_L and σ_N are defined as

$$\sigma_L = \frac{\sum_{(m,n)\in L_1} \lambda_2\,(m,n)}{\mathrm{num}\,((m,n) \in L_1)} \tag{11}$$

$$\sigma_N = \frac{\sum_{(m,n)\in N} \lambda_2\,(m,n)}{\mathrm{num}\,((m,n) \in N)} \tag{12}$$

where the operation $\mathrm{num}(\cdot)$ represents the number of elements that meet the condition in parentheses. Then, the layover area L_2 marked by eigenvalue is

$$L_2 = \{(m,n) \in s_0 | \mathrm{num}(\boldsymbol{\lambda}\,(m,n) > \sigma_N) \geq 2\}\,. \tag{13}$$

Based on the above analysis, finally, the pixel (m,n) is judged as a layover pixel in the following three situations:

1) The pixel (m,n) is directly marked as layover when it is contained in both L_1 and L_2:
$$L_3 = \{(m,n) \in s_0 |\,(m,n) \in L_1\ and\ (m,n) \in L_2)\}\,. \tag{14}$$
2) When pixel (m,n) is marked in L_1, but not marked in L_2, a further judgment is made and the final layover is L_4:
$$L_4 = \Bigg\{ (m,n) \in s_0 |\,(m,n) \in L_1\ and\ (m,n) \notin L_2\ and\ \lambda_2\,(m,n) > \frac{\sigma_L + \sigma_N}{2}\,) \Bigg\}. \tag{15}$$
3) When pixel (m,n) is marked in L_2, but not marked in L_1, a further judgment is made and the final layover is L_5:
$$L_5 = \Bigg\{ (m,n) \in s_0\,|(m,n) \in L_2\ and\ (m,n) \notin L_1\ and\ \lambda_2\,(m,n) > \frac{\sigma_L + \sigma_N}{2}\,) \Bigg\} \tag{16}$$

The flowchart of the joint detection method is shown in Fig. 3 and the implementation is as follows.

A. Selection of Common Master Image and Registration

The joint correlation coefficient is calculated when each image is used as the common master image. The acquisition with

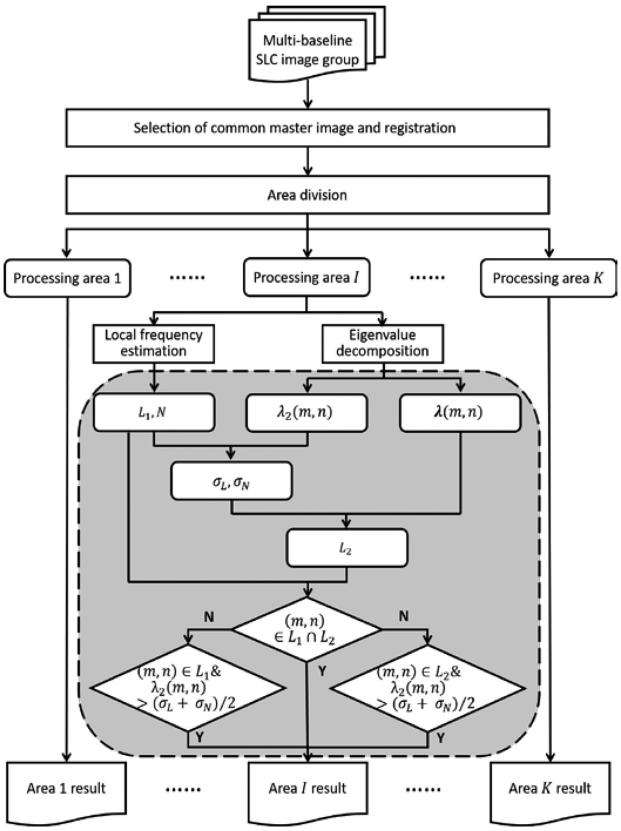

Fig. 3. Flowchart of joint detection method of multibaseline InSAR.

the largest joint correlation coefficient will be selected as the common master image [38]. The master and slave images are registered by the correlation coefficient method [39].

B. Area Division

The whole image is partitioned into different areas which contain layovers according to the SAR amplitude of the master image, that is, areas with high-amplitude pixels.

Assuming that there are altogether K partitioned areas, the following procedures all take Area I as an example. The other areas are processed in the same manner as Area I.

C. Local Frequency Estimation on Maximum Likelihood Fusion Phase

Complex conjugate multiplication is performed on the master and slave images to obtain the interferogram. The reference terrain phase, fitting through control points [33], is removed to obtain the flattened interferometric phase. Then, phase filtering [34] is applied to the flattened interferograms.

Usually, the longest baseline is chosen as a referred baseline. The unwrapped phase of the shortest baseline is stretched into the scale of the long baseline, and the scaled result is set as the search center of the maximum likelihood fusion. The interferometric phases of all baselines in the search interval are substituted into (5). The maximum likelihood fusion phase is then taken as the phase corresponding to the maximum of likelihood function. The local frequency estimation using 2-D FFT and CZT is applied to the maximum likelihood fusion phase to obtain $f_{\mathrm{r,\ CZT}}(m,n)$ for each pixel.

D. Eigenvalue Decomposition After Adaptive Image Selection

According to the correlation coefficient histogram, the SLC SAR image set is selected for Area I. For each pixel in Area I, eigenvalue decomposition is performed on the signal covariance matrix to get $\lambda_2(m,n)$. At the same time, the eigenvalue vector $\boldsymbol{\lambda}(m,n)$ is kept for layover detection later.

E. Joint Detection

First, (9) and (10) are used to define L_1 and N. Next, the thresholds σ_L and σ_N for joint detection are calculated by (11) and (12). Meantime, the layover L_2 can be marked according to the eigenvalue vectors using (13). Finally, the layover detection results $L_1,\ L_2$ and the thresholds $\sigma_L,\ \sigma_N$ are used for joint judgment. Using (14)–(16), the final layover marked by joint detection is determined as $L_3 \cup L_4 \cup L_5$.

For the local frequency method, it needs additional information to distinguish layover and shadow. The proposed joint detection provides eigenvalue to deal with the problem. For the eigenvalue method, the boundary between signal and noise eigenvalues is usually blurred because of noise. Although filtering enables highlighting the boundary, it is still inevitably affected by noise [14]. In our proposed joint detection, the layover detected by local frequency is used as *a priori* condition for eigenvalue judgment, and the more robust results are obtained for the number of larger eigenvalues. So the joint detection based on local frequency and eigenvalue is more superior.

IV. Experiments and Analysis

In this section, the proposed method is validated through three experiments. The first two experiments show the feasibility of the multibaseline methods proposed in Section II. In the third experiment, both simulated data and real data are processed to verify the joint detection method in comparison to the single-feature methods. The performance of layover detection is quantitatively analyzed by this two metrics: false alarm, which indicates the layover misjudgment in all pixels, and accuracy, which shows the proportion of detected layover pixels.

A. Details of Experimental Data

Both simulated and real data are processed to validate the proposed method. The simulation employs an existing DEM dataset, the Advanced Spaceborne Thermal Emission and Reflection Radiometer (ASTER) DEM [40]. The system parameters of simulation refer to TanDEM-X [8]. The baseline lengths of the multibaseline InSAR are [200 220 240 260 300 320] m. The added Gaussian white noise makes the signal-to-noise ratio equal to 5 dB. The true value of the layover area is estimated by calculating the terrain slope of the ASTER DEM only in the range direction. The terrain slope angle is calculated as the height gradient divided by the pixel size in the range direction. Layover occurs where the slope angle is larger than the incidence angle

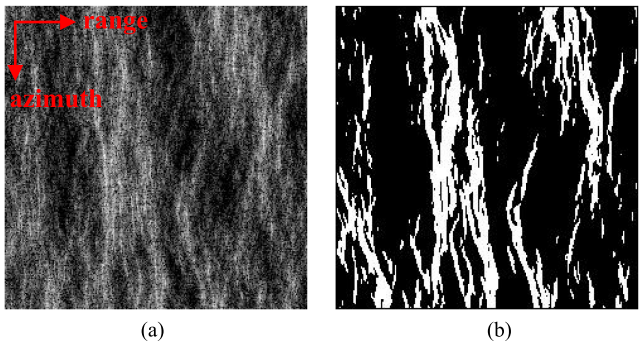

Fig. 4. Visual representation of the simulated data. (a) SAR amplitude image. (b) True value of the layover area.

TABLE I
SYSTEM PARAMETERS OF REAL DATA

Parameters	Value
Wavelength	0.03125 m
Near range	511.5 km
Slant range resolution	2.79 m
Azimuth resolution	3.3 m
Incidence angle	35.09°
Baseline range	-179.4851 – 313.3913 m

[41], [42]. The SAR amplitude image of the simulation scene and the true value of the layover area are illustrated in Fig. 4.

Comparative experiments are also conducted on real data. A set of 31 multibaseline data obtained by the TerraSAR-X satellite is processed. The acquisitions are taken from January 22, 2012 to February 4, 2016 over the city of Beijing, China. The parameters of the acquisitions are listed in Table I. SAR data of two regions are used for layover detection. Region 1 is located near Beijing Capital International Airport. Its optical image is shown in Fig. 5(a), and its SAR amplitude image with a 512 × 512 sample dimension is shown in Fig. 5(b). Region 2 is located near the Bjxiangsu Community. Its optical image is shown in Fig. 5(c), and its SAR amplitude image with a 900 × 500 sample dimension is shown in Fig. 5(d).

B. Experiments and Result Analysis

1) Local Frequency Estimation: The first experiment demonstrates the effectiveness of the multibaseline local frequency estimation by maximum likelihood phase fusion introduced in Section II-B. The 200 m baseline is treated as the short baseline, and the other baselines are regarded as the long baseline to form five baseline combinations, as shown in Table II.

Initially, the estimation precision of the long-baseline interferometric phase and the maximum likelihood phase is compared. Minimum cost flow phase unwrapping [43] is applied to unwrap the phases, and the unwrapped phases are used for phase fusion. The estimation results are evaluated with two metrics. One is the standard deviation of phase error (SDP) and the other is the standard deviation of local frequency error (SDF). The SDP and

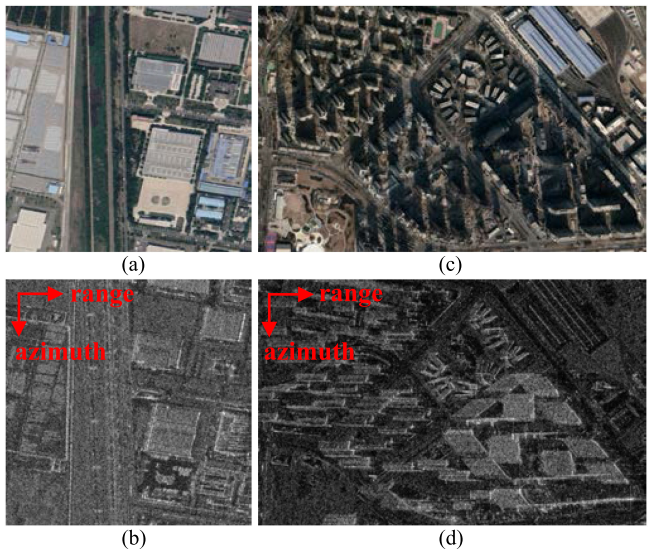

Fig. 5. Visual representation of the real data. (a) (Top left) Optical image of Region 1, located near Beijing Capital International Airport. (b) (Bottom left) SAR amplitude image of Region 1 with a 512 × 512 sample dimension. (c) (Top right) Optical image of Region 2, located near the Bjxiangsu Community. (d) (Bottom right) SAR amplitude image of Region 2 with a 900 × 500 sample dimension.

TABLE II
SDP AND SDF OF LOCAL FREQUENCY ESTIMATION

Baseline combination	Long-baseline		Maximum likelihood	
	SDP	SDF	SDP	SDF
200 – 220m	0.4955	0.0421	0.4791	0.0407
200 – 240m	0.5175	0.0456	0.5034	0.0432
200 – 260m	0.5545	0.0523	0.5409	0.0487
200 – 300m	0.6240	0.0610	0.6099	0.0566
200 – 320m	0.6467	0.0635	0.6417	0.0591

SDP is short for the standard deviation of phase error and SDF is short for the standard deviation of local frequency error.

SDF are calculated as follows [32]:

$$\mathrm{SDP} = \sqrt{\frac{1}{C-1}\sum_{c=1}^{C}\left(\Delta\phi\left(m_c,n_c\right)-\overline{\Delta\phi}\right)^2} \tag{17}$$

$$\mathrm{SDF} = \sqrt{\frac{1}{C-1}\sum_{c=1}^{C}\left(\Delta f\left(m_c,n_c\right)-\overline{\Delta f}\right)^2} \tag{18}$$

where C is the number of pixels. $\Delta\phi\ (m,n) = \phi(m,n) - \phi_{\mathrm{true}}(m,n)$. In which, $\phi_{\mathrm{true}}(m,n)$ is the true value of the long-baseline interferometric phase; $\phi(m,n)$ is the long-baseline phase or the maximum likelihood phase; $\overline{\Delta\phi}$ is the average of the phase error $\Delta\phi$. $\Delta f\ (m,n) = f(m,n) - f_{\mathrm{true}}(m,n)$. In which, $f_{\mathrm{true}}(m,n)$ is the true value of the local frequency; $f(m,n)$ is the local frequency of the long-baseline phase or the local frequency of maximum likelihood phase; and $\overline{\Delta f}$ is the average of the local frequency error Δf.

The SDP and SDF of the five baseline combinations are shown in Table II. By comparing SDP, it can be seen that the maximum

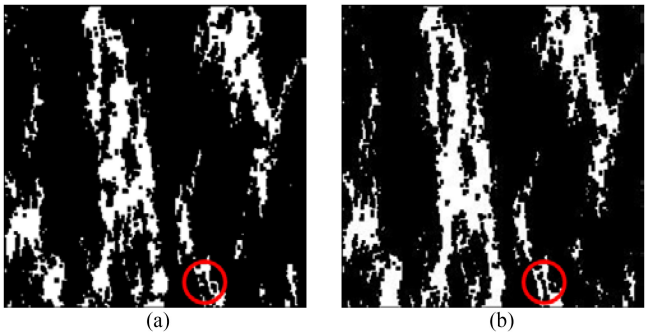

Fig. 6. Layover detection results with long-baseline phase and maximum likelihood phase. (a) Layover area detected by local frequency estimation on long-baseline phase. (b) Layover area detected by local frequency estimation on maximum likelihood phase. The red circle shows a detail which is detected in (b) but not in (a).

TABLE III
LAYOVER DETECTION RESULT USING LOCAL FREQUENCY

Baseline combination	Long-baseline			Maximum likelihood		
	False alarm	Accuracy	Time	False alarm	Accuracy	Time
200 – 220m	0.0087	0.5953	9.34s	0.0091	0.6419	18.29s
200 – 240m	0.0088	0.6007	9.35s	0.0093	0.6557	18.31s
200 – 260m	0.0076	0.5649	9.36s	0.0087	0.6421	18.30s
200 – 300m	0.0074	0.5300	9.34s	0.0086	0.6400	18.28s
200 – 320m	0.0074	0.5144	9.35s	0.0086	0.6392	18.31s

likelihood phase combining both the short-baseline and the long-baseline data helps estimate the interferometric phase more precisely. Simultaneously, the comparison of SDF proves that the estimation precision of corresponding local frequency is also improved.

Then, the local frequency estimated by the long-baseline phase and the maximum likelihood phase are used to perform layover detection. Fig. 6 shows the detection results. Comparing with the true value of layover area shown in Fig. 4(b), the result corresponding to the maximum likelihood phase marks the correct detail in the red circle, which is missed in the result of the long-baseline phase. The layover detection results of the five baseline combinations in Table III also prove the superiority of layover detection using the maximum likelihood phase of multibaseline InSAR.

The runtime of layover detection based on the long-baseline phase and that based on the maximum likelihood phase using MATLAB R2018b are listed in Table III. The parallel computing toolbox along with multicore CPUs is employed. Due to the phase fusion based on maximum likelihood estimation, the runtime of the proposed multibaseline local frequency estimation is longer than that of the existing single-baseline method.

2) Eigenvalue Decomposition: The second experiment aims to validate the superiority of adaptive selection of SLC SAR images based on coherence for multibaseline eigenvalue decomposition.

First, the joint correlation coefficient is calculated when each image is served as the common master image. The 14th SLC SAR image is eventually selected as the master image. Then, as

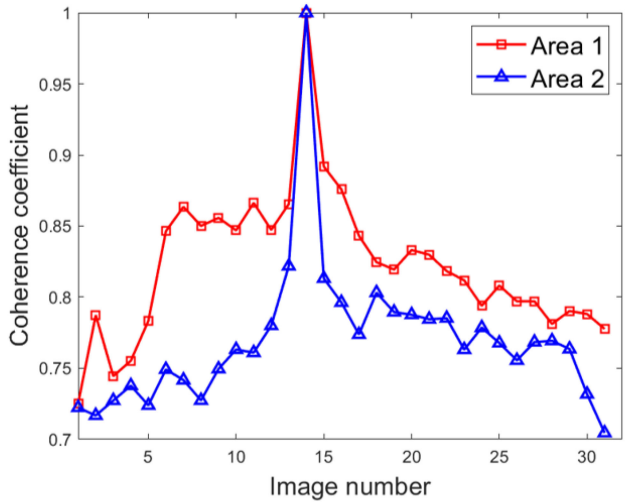

Fig. 7. Correlation coefficients of the 30 image pairs. The 14th SLC SAR image is chosen as the master image. The red line represents Area 1, with the SAR amplitude image shown in Fig. 9(a). The blue line represents Area 2, with the SAR amplitude image shown in Fig. 9(b).

an example, Area 1 and Area 2 are partitioned from Region 1 shown in Fig. 5(b), as shown in Fig. 9. The correlation coefficients of 30 image pairs are calculated for Area 1 and Area 2, as shown in Fig. 7. It can be seen that the correlation coefficients are quite different from one area to another. For instance, the 18th and the 19th slave images have higher coherence in Area 2, while lower coherence in Area 1. Hence, different images should be selected for different divided areas. The statistical histograms of the correlation coefficients for Area 1 and Area 2 are used to determine the threshold of the SLC SAR image selection, as shown in Fig. 8, respectively. There are double peaks in the histograms, and the correlation coefficient located in the trough of the double peaks is chosen as the threshold. The threshold of Area 1 is 0.8370 and the threshold of Area 2 is 0.7715.

Using the proposed image selection method, the selected image set for Area 1 is [14 15 16 11 13 7 9 8 12 10 6 17] and that for Area 2 is [14 13 15 18 16 19 20 22 21 12 24 17].

To verify the effectiveness of the proposed adaptive image selection, the other four image sets for Area 1 and Area 2 are also used to perform layover detection with result comparison, respectively, where the image set (v) [1]–[31] is the case of the previous study.

Area 1: (i) [14 15 16 11 13 7 9 8]; (ii) [14 15 16 11 13 7 9 8 12 10 6 17]; (iii) [1–8]; (iv) [1–12]; (v) [1–31].
Area 2: (i) [14 13 15 18 16 19 20 22]; (ii) [14 13 15 18 16 19 20 22 21 12 24 17]; (iii) [1–8]; (iv) [1–12]; (v) [1–31].

Among them, the comparison of (i), (ii), (v) is used to study the pros and cons of increasing the number of image samples. The comparison of (i), (iii) and that of (ii), (iv) are used to study the impact of coherence on the detection results under the same number of samples. The layover detection results with eigenvalue decomposition are shown in Fig. 9.

Comparing the results of (i), (ii), the outline of the result (ii) is more precise. This indicates that increasing the number of image

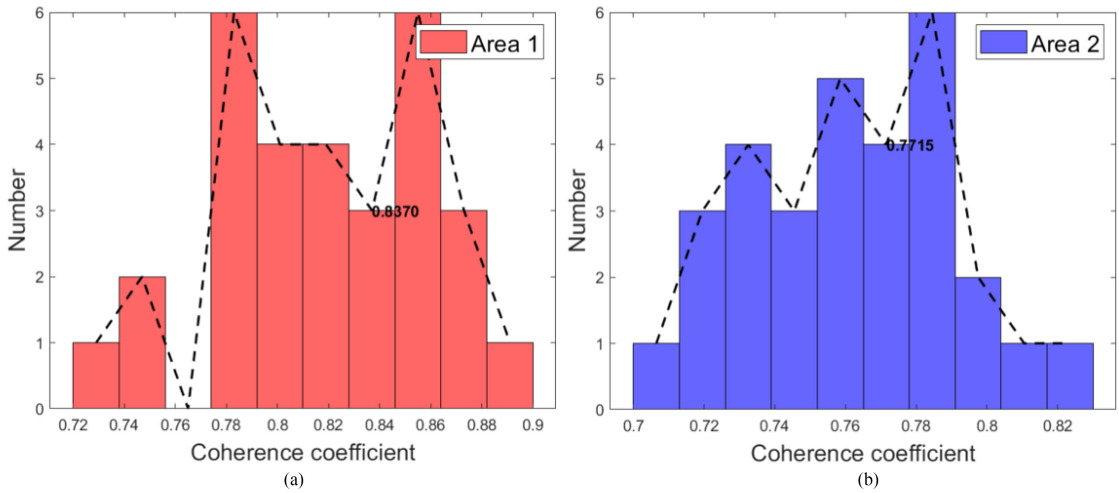

Fig. 8. Statistical histograms of the correlation coefficients. The statistical histogram on the left represents Area 1. The statistical histogram on the right represents Area 2. The threshold for SLC SAR image selection is 0.8370 for Area 1 and 0.7715 for Area 2.

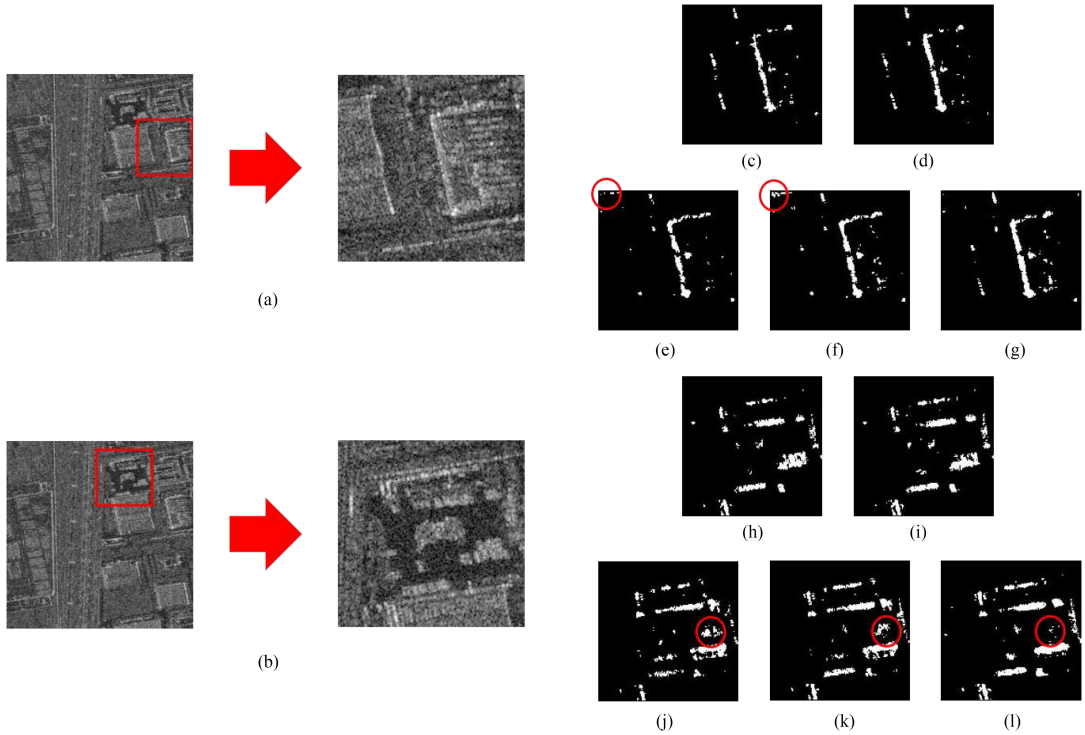

Fig. 9. Comparative experiment results using eigenvalue decomposition. (a) shows the SAR amplitude image of Area 1, (b) shows the SAR amplitude image of Area 2. (c), (d), (e), (f), (g) show the detection result of (i)–(v) in Area 1, (h), (i), (j), (k), (l) show the detection result of (i)–(v) in Area 2, respectively. The normal area indicated by the red circle is misjudged as the layover area. Blindly increasing the number of images used will also bring disadvantages.

samples will result in better detection results when the coherence is more significant than a certain threshold. Comparing the results of (i), (ii), (v) of Area 2, the normal area indicated by the red circle is misjudged as a layover in (v), which shows that due to the use of low coherence images, there is a cross-blur between signal eigenvalues and noise eigenvalues.

It can be seen from the results of (i), (iii) and (ii), (iv) that there are more misjudgments in (iii), (iv), which shows that the combination with strong coherence has better performances in terms of false alarm and accuracy with the same number of samples.

Based on the above theoretical analysis and experimental results, the following conclusions are drawn:

1) Increasing the number of image samples could benefit the eigenvalue decomposition and the subsequent layover detection. However, introducing image samples with low coherence may negatively influence the decomposition and detection.

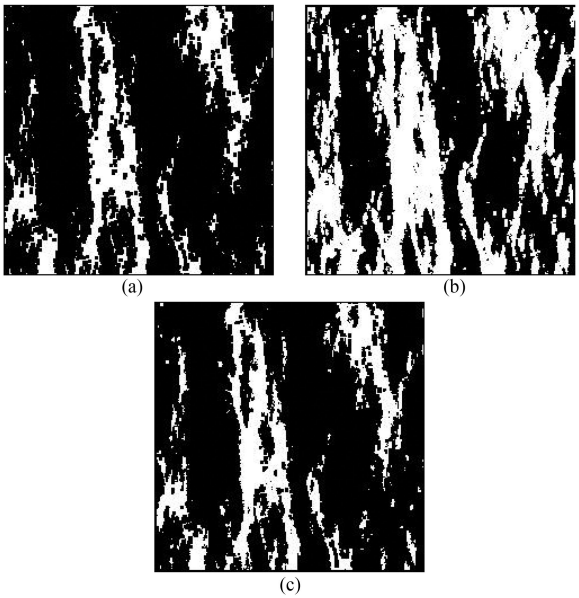

Fig. 10. Layover detection result on simulated data. (a) Layover area detected by local frequency estimation on the maximum likelihood estimation. (b) Layover area detected by multibaseline eigenvalue decomposition. (c) Layover area detected by the proposed joint detection method.

TABLE IV
LAYOVER DETECTION RESULT OF SIMULATED DATA

Method	False alarm	Accuracy	Time
Local frequency estimation	0.0093	0.6557	18.31s
Eigenvalue decomposition	0.0380	0.9315	6.91s
Joint detection	0.0096	0.7466	25.28s

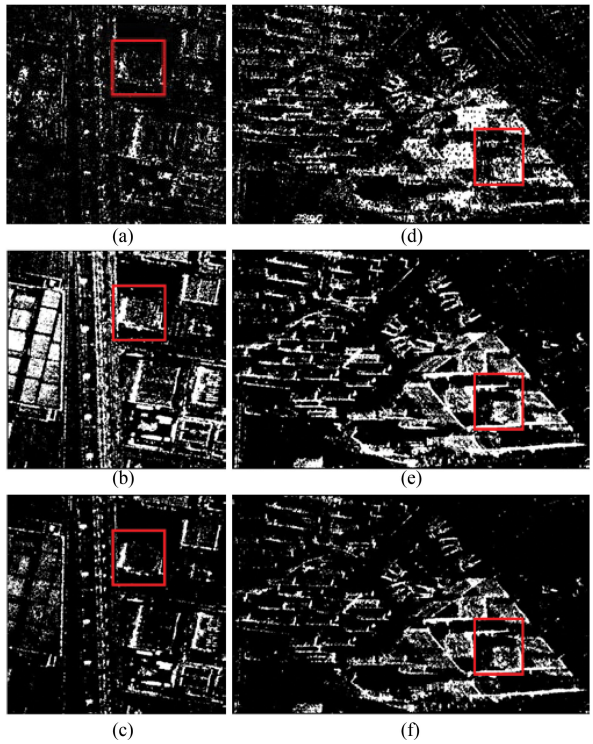

Fig. 11. Layover detection results on real data. (a) Layover area detected by multibaseline local frequency estimation on Region 1. (b) Layover area detected by multibaseline eigenvalue decomposition on Region 1. (c) Layover area detected by the joint detection proposed on Region 1. (d) Layover area detected by multibaseline local frequency estimation on Region 2. (e) Layover area detected by multibaseline eigenvalue decomposition on Region 2. (f) Layover area detected by the joint detection proposed on Region 2. Located near Beijing Capital International Airport, the buildings in Region 1 are all low-rise buildings with a height of fewer than 10 m. Region 2 is delineated in the Bjxiangsu Community. According to the community information, the estate's average height is 60–70 m.

2) Coherence is the main factor in image selection, and the image set with strong coherence can reduce false alarms and improve accuracy.
3) The selection of images is related to the ground scene, and the effectiveness of the proposed adaptive image selection method is verified.

For Region 1, the runtime of layover detection using the 12 selected images is 41.74 s, while that using all 31 images is 76.00 s. It can be seen that the proposed adaptive selection of SLC SAR images not only improves the estimation precision but also enhances the computational efficiency. Thus, it is necessary to select the suitable images with the proposed adaptive selection of SLC SAR images before multibaseline InSAR eigenvalue decomposition.

3) Layover Detection: In this part, through comparative experiments on simulated data and real data, the proposed multibaseline joint detection method based on local frequency and eigenvalue is tested against detection with multibaseline local frequency estimation and multibaseline eigenvalue decomposition.

First, the results of the simulated data are analyzed. The true value of the layover area is shown in Fig. 4(b). The detected layover areas are shown in Fig. 10. The false alarm and accuracy are listed in Table IV.

In comparison with joint detection, more layover pixels are missed in the result of local frequency estimation because a high amplitude threshold is required to distinguish layover from the other abnormal areas such as the shadow. The false alarm of the layover detection using multibaseline eigenvalue decomposition is relatively high. This is because the average of the second eigenvalues of the normal area is set as the threshold of the eigenvalue decomposition, and the normal area is partially misjudged as the layover area. Joint detection uses local frequency estimation and eigenvalue decomposition to set precise thresholds. It then combines the layover detected by local frequency, the layover detected by eigenvalue and the thresholds for joint judgment. The accuracy is improved as well as the false alarm is relatively few.

The runtime of these methods is listed in Table IV. In addition to local frequency estimation and eigenvalue decomposition, joint judgment is performed in the joint detection method. Thus, its time expense is larger than the others, as shown in Table IV. However, there is little substantial workload of calculation beyond the sum of the other two methods.

The following is an application of the proposed method to real data. There is no true value of the layover area for real data, so the result can only be qualitatively analyzed through optical

images and SAR amplitude images. Fig. 11 shows the detection results of Region 1 and Region 2. The subfigures from top to bottom illustrate the result based on local frequency, based on eigenvalue, and based on joint detection, respectively.

In practice, the building layover comprises of several contributors such as ground, wall, and window eaves. It appears as a brighter area in the SAR amplitude image. Located near Beijing Capital International Airport, the buildings in Region 1 shown in Fig. 5(a) are all factories, including The Beijing No. 1 Machine Tool Plant. They are all low-rise buildings with a height of fewer than 10 m. Therefore, there are few layover areas on the roof. The layover areas are mainly concentrated on the edge of the building. The red box shows a low-rise building. The local frequency estimation result shown in Fig. 11(a) does not maintain the roof edge, while the eigenvalue decomposition result shown in Fig. 11(b) mistakenly detects the roof as layover. Region 2 shown in Fig. 5(c) is delineated in the Bjxiangsu Community. According to the community information, the estate's average height is 60–70 m, so there are many overlapping spots on the roof. It can be seen from the red box comparison in the subfigures, Fig. 11(d) misses a building parallel to the azimuth direction while the roof edge in Fig. 11(e) has spread. Thus, joint detection obtains the most reliable layover detection result.

V. Conclusion

The layover area in SAR interferograms affects the subsequent InSAR processing, such as interferometric phase filtering and phase unwrapping. Therefore, the layover needs to be detected in advance. The application scenarios of existing layover detection methods are mostly for single-baseline InSAR, which exhibit high false alarm and low accuracy. Multibaseline InSAR provides more image samples, thus further improves the precision of layover detection. Among the published articles, only Chen *et al.* in our research team have conducted study on layover detection of multibaseline InSAR only with eigenvalue where all available images are used to estimate the eigenvalue without data choosing.

A novel layover joint detection method is proposed for multibaseline InSAR. It combines local frequency and eigenvalue of multibaseline InSAR to exploit the multibaseline InSAR advantages and obtain more precise layover detection. For multibaseline InSAR, the flattened interferometric phase fusion based on maximum likelihood is given for local frequency estimation and the adaptive image selection is presented for eigenvalue decomposition. The theoretical analysis and experimental results show the feasibility and superiority of our proposed joint detection method of multibaseline InSAR.

Acknowledgment

The dataset is provided by Geospatial Data Cloud site, Computer Network Information Center, Chinese Academy of Sciences.[1]

[1][Online]. Available: http://www.gscloud.cn

References

[1] A. Moreira, P. Prats-Iraola, M. Younis, G. Krieger, I. Hajnsek, and K. P. Papathanassiou, "A tutorial on synthetic aperture radar," *IEEE Geosci. Remote Sens. Mag.*, vol. 1, no. 1, pp. 6–43, Mar. 2013.

[2] M. Pichierri, B. Rabus, and I. Hajnsek, "Single-baseline polarimetric SAR interferometry for characterizing the biophysical properties of agricultural crops," in *Proc. IEEE Int. Geosci. Remote Sens. Symp.*, 2017, pp. 3882–3889.

[3] H. Wang, K. Ouchi, and Y. Jin, "Classification of typhoon-destroyed forests based on tree height change detection using InSAR technology," in *Proc. IEEE Int. Geosci. Remote Sens. Symp.*, 2011, pp. 1247–1250.

[4] F. Cigna and D. Tapete, "Sentinel-1 InSAR assessment of present-day land subsidence due to exploitation of groundwater resources in central Mexico," in *Proc. IEEE Int. Geosci. Remote Sens. Symp.*, 2020, pp. 4215–4218.

[5] S. Baek and C. K. Shum, "Antarctic ocean tide signal restoration using differential InSAR technique," in *Proc. 3rd Int. Asia-Pacific Conf. Synthetic Aperture Radar*, 2011, pp. 1–4.

[6] A. Moreira *et al.*, "Multi-baseline spaceborne SAR imaging," in *Proc. IEEE Int. Geosci. Remote Sens. Symp.*, 2016, pp. 1420–1423.

[7] A. Ferretti, C. Prati, and F. Rocca, "Permanent scatterers in SAR interferometry," in *Proc. IEEE Int. Geosci. Remote Sens. Symp.*, 1999, pp. 1528–1530.

[8] G. Krieger *et al.*, "TanDEM-X: A satellite formation for high-resolution SAR interferometry," *IEEE Trans. Geosci. Remote Sens.*, vol. 45, no. 11, pp. 3317–3341, Nov. 2007.

[9] X. X. Zhu and R. Bamler, "Superresolving SAR tomography for multidimensional imaging of urban areas: Compressive sensing-based TomoSAR inversion," *IEEE Signal Process. Mag.*, vol. 31, no. 4, pp. 51–58, Jul. 2014.

[10] M. Zink *et al.*, "TanDEM-X: The new global DEM takes shape," *IEEE Geosci. Remote Sens. Mag.*, vol. 2, no. 2, pp. 8–23, Jun. 2014.

[11] A. Reigber and A. Moreira, "First demonstration of airborne SAR tomography using multibaseline L-band data," *IEEE Trans. Geosci. Remote Sens.*, vol. 38, no. 5, pp. 2142–2152, Sep. 2000.

[12] M. Eineder, "Problems and solutions for InSAR digital elevation model generation of mountainous terrain," *J. Neurochem.*, 2003.

[13] J. Guo, Z. Li, and Z. Bao, "Using multibaseline InSAR to recover layovered terrain considering wideband array problem," *IEEE Geosci. Remote Sens. Lett.*, vol. 5, no. 4, pp. 583–587, Apr. 2008.

[14] L. Wei, T. Balz, M. Liao, and L. Zhang, "TerraSAR-X stripmap data interpretation of complex urban scenarios with 3D SAR tomography," *J. Sensors*, vol. 2014, Oct. 2014, Art. no. 386753.

[15] U. Soergel, K. Schulz, and U. Thoennessen, "Enhancement of interferometric SAR data using segmented intensity information in urban areas," in *Proc. IEEE Int. Geosci. Remote Sens. Symp.*, 2000, pp. 3216–3218.

[16] W. He, M. Jager, and O. Hellwich, "Comparison of three unsupervised segmentation algorithms for SAR data in urban areas," in *Proc. IEEE Int. Geosci. Remote Sens. Symp.*, 2008, pp. 241–244.

[17] X. Qin, S. Zhou, H. Zou, and Y. Ren, "A CFAR algorithm for layover and shadow detection in InSAR images based on kernel density estimation," in *Proc. 5th Int. Conf. Digit. Image Process.*, 2013, p. 42.

[18] J. Yu, M. Wu, C. Li, and S. Zhu, "A SAR image segmentation method based on otsu and level set," in *Proc. IEEE 9th Joint Int. Inf. Technol. Artif. Intell. Conf.*, 2020, pp. 2189–2193.

[19] C. Prati and F. Rocca, "Improving slant-range resolution with multiple SAR surveys," *IEEE Trans. Aerosp. Electron. Syst.*, vol. 29, no. 1, pp. 135–143, Jan. 1993.

[20] F. Gatelli, A. M. Guamieri, F. Parizzi, P. Pasquali, C. Prati, and F. Rocca, "The wavenumber shift in SAR interferometry," *IEEE Trans. Geosci. Remote Sens.*, vol. 29, no. 8, pp. 855–865, Aug. 1994.

[21] D. Petit, F. Adragna, and J.-D. Durou, "Filtering of layover areas in high-resolution IFSAR for building extraction," in *Proc. Europto Remote Sens.*, 2000, pp. 230–240.

[22] W. Liu, K. Suzuki, and F. Yamazaki, "Height estimation for high-rise buildings based on InSAR analysis," in *Proc. Joint Urban Remote Sens. Event*, 2015, pp. 1–4.

[23] C. Rossi and M. Eineder, "High-resolution InSAR building layovers detection and exploitation," *IEEE Trans. Geosci. Remote Sens.*, vol. 53, no. 12, pp. 6457–6468, Dec. 2015.

[24] M. Wax and T. Kailath, "Detection of signals by information theoretic criteria," *IEEE Trans. Acoust. Speech Signal Process.*, vol. 33, no. 2, pp. 387–392, Apr. 1985.

[25] H. Zou, B. Cai, C. Fan, and R. Yun, "Layover and shadow detection based on distributed spaceborne single-baseline InSAR," *Signal Process.*, vol. 17, no. 1, 2010, Art. no. 012243.

[26] W. Chen, H. Xu, and S. Li, "A novel layover and shadow detection method for InSAR," in *Proc. IEEE Int. Conf. Imag. Syst. Techn.*, 2013, pp. 441–445.
[27] X. Du, Q. Yang, B. Cai, and D. Liang, "A new method on shadow and layover detection of InSAR," in *Proc. 6th Asia-Pacific Conf. Antennas Propag.*, 2017, pp. 1–3.
[28] S. Wang, H. Xu, B. Yang, and Y. Luo, "Improved InSAR layover and shadow detection using multi-feature," in *Proc. IEEE Int. Geosci. Remote Sens. Symp.*, 2020, pp. 28–31.
[29] R. Hanssen, *Radar Interferometry: Data Interpretation and Error Analysis*. Dordrecht, The Netherlands: Kluwer Academic Publishers, 2001.
[30] P. A. Rosen *et al.*, "Synthetic aperture radar interferometry," *Proc. IEEE*, vol. 88, no. 3, pp. 333–382, Mar. 2000.
[31] H. Yu, Y. Lan, Z. Yuan, J. Xu, and H. Lee, "Phase unwrapping in InSAR: A review," *IEEE Geosci. Remote Sens. Mag.*, vol. 7, no. 1, pp. 40–58, Mar. 2019.
[32] H. Xu, S. Li, Y. You, A. Liu, and W. Liu, "Unwrapped phase estimation via normalized probability density function for multibaseline InSAR," *IEEE Access*, vol. 7, pp. 4979–4988, 2019.
[33] C. Lin, L. Chen, and S. Ge, "Research on method of flat earth effect removal based on refined local fringe frequency," in *Proc. IET Int. Radar Conf.*, 2013, pp. 1–6.
[34] D. Y. Zhu, Z. D. Zhu, and Q. C. Xie, "A topography adaptive interferogram filter based on local frequency estimation," *Acta Acta Electronica Sinica*, vol. 30, pp. 1853–1856, 2002.
[35] N. K. Kottayil, A. Zimmer, S. Mukherjee, X. Sun, P. Ghuman, and I. Cheng, "Accurate pixel-based noise estimation for InSAR interferograms," in *Proc. IEEE SENSORS*, 2018, pp. 1–4.
[36] Z. Tang, Y. Zhou, and J. Li, "Study on co-registration method based on correlation coefficient for InSAR signal processing," in *Proc. IEEE Int. Geosci. Remote Sens. Symp.*, 2005, pp. 3867–3870.
[37] A. J. Wilkinson, "Synthetic aperture radar interferometry: A model for the joint statistics in layover areas," in *Proc. South Afr. Symp. Commun. Signal Process.*, 1998, pp. 333–338.
[38] Z. Zhengwei and Z. Jianjiang, "Optimum selection of common master image for ground deformation monitoring based on PS-DInSAR technique," *J. Syst. Eng. Electron.*, vol. 20, no. 6, pp. 1213–1220, 2009.
[39] N. Yagüe-Martínez *et al.*, "Interferometric processing of Sentinel-1 TOPS data," *IEEE Trans. Geosci. Remote Sens.*, vol. 54, no. 4, pp. 2220–2234, Apr. 2016.
[40] H. Fujisada, F. Sakuma, A. Ono, and M. Kudoh, "Design and preflight performance of ASTER instrument protoflight model," *IEEE Trans. Geosci. Remote Sens.*, vol. 36, no. 4, pp. 1152–1160, Jul. 1998.
[41] X. Zhang, Q. Zeng, J. Jiao, and J. Zhang, "Fusion of space-borne multibaseline and multi-frequency interferometric results based on extended Kalman filter to generate high quality DEMs," *ISPRS J. Photogramm.*, vol. 111, pp. 32–44, 2016.
[42] R. A. Mcdonnell, C. Lloyd, and P. Burrough, *Principles of Geographical Information Systems*. Oxford, U.K.: Oxford Univ. Press, 1998.
[43] M. Costantini, "A novel phase unwrapping method based on network programming," *IEEE Trans. Geosci. Remote Sens.*, vol. 36, no. 3, pp. 813–821, Mar. 1998.

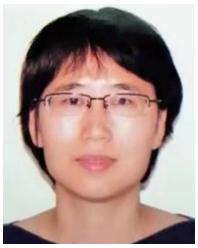

Huaping Xu (Member, IEEE) received the B.S. degree in electronic engineering and the Ph.D. degree in communication and information system from Beihang University, Beijing, China, in 1998 and 2003, respectively.

She is currently a Professor with the School of Electronic and Information Engineering, Beihang University. She has now authored/coauthored more than 100 journal and conference papers, and a research monograph about signal processing. Her research interests include synthetic aperture radar interferometry, differential SAR interferometry, image processing, and radar waveform design.

Siyuan Wang received the B.S. degree in information and computing science from Beihang University, Beijing, China, in 2018, where she is currently working toward the M.S. degree in system engineering.

Her research interests include SAR interferometry, multibaseline SAR, and image processing.

Shuo Li received the M.S. degree in electronic science and technology from China University of Mining and Technology, Xuzhou, China, in 2015. He is currently working toward the Ph.D. degree in signal and information processing with Beihang University, Beijing, China.

His research interests include SAR image processing, SAR interferometry processing, especially registration and phase unwrapping.

Guobing Zeng received the B.S. degree in aircraft engineering from Beihang University, Beijing, China, in 2019. He is currently working toward the Ph.D. degree in signal and information processing with the School of Electronic and Information Engineering, Beihang University.

His research interests include SAR interferometry and differential SAR interferometry.

Zhenwan You received the B.S. degree in electronic information engineering from Central South University, Changsha, China, in 2019. He is currently working toward the M.S. degree in electronic and communication engineering with the School of Electronic and Information Engineering, Beihang University, Beijing, China.

His research interest includes SAR interferometry processing.

Wei Li received the Ph.D. degree in signal and information processing from Beihang University, Beijing, China, in 2011.

He is currently a Senior Engineer with the Shanghai Institute of Satellite Engineering, Shanghai, China. He is currently a Member of the National Space Infrastructure Demonstration Group and Secretary General of the Secretariat of the Civil P-Band Satellite Scientists Committee. His research interests include satellite system design and system performance analysis.